0026-895X/06/6905-1534–1541$20.00
MOLECULAR PHARMACOLOGY
Vol. 69, No. 5
20107/3104200

Mol Pharmacol 69:1534–1541, 2006
Printed in U.S.A.

Liver Deformation in *Ahr*-Null Mice: Evidence for Aberrant Hepatic Perfusion In Early Development

Eric B. Harstad, Christopher A. Guite, Tami L. Thomae, and Christopher A. Bradfield

McArdle Laboratory for Cancer Research, University of Wisconsin Medical School, Madison, Wisconsin

Received October 19, 2005; accepted January 27, 2006

ABSTRACT

Mice harboring mutations in the *Ahr* locus display a patent ductus venosus and smaller livers throughout life. We tested the hypothesis that these hepatic aberrations are secondary to a developmental defect in hepatovascular blood flow by performing a detailed analysis of hepatic development in wild-type and $Ahr^{-/-}$ mice. This study revealed necrotic lesions in the peripheries of $Ahr^{-/-}$ fetal livers as early as embryonic day 15.5, with an increasing incidence up to postnatal day 1 and resolution by 2 weeks post partum. To visualize perfusion of fetal livers, we injected fluorescein isothiocyanate-labeled dextran into the cranial artery and monitored hepatic fluorescence by microscopy. The peripheries of the median and left lobes displayed decreased perfusion in regions corresponding to those regions that displayed necrosis at later developmental times. An examination of adult $Ahr^{-/-}$ animals revealed that smaller livers are predominantly due to decreased sizes of the left and right lobes, corresponding to regions of decreased perfusion and hepatic necrosis observed in fetal livers. Histological aberrations in the portal vein also support a model in which perfusion is compromised in the $Ahr^{-/-}$ liver. Taken in sum, these results indicate that the *Ahr* locus is required for normal perfusion of the developing liver and that disruption of the AHR signaling pathway gives rise to fetal hepatic necrosis and consequent liver deformation which persists through adulthood.

The aryl hydrocarbon receptor (AHR) is a ligand-activated member of the Per-Arnt-Sim (PAS) superfamily of transcription factors. This protein has long been studied for its role as the receptor for polycyclic aromatic hydrocarbon and halogenated-dioxin ligands (Gu et al., 2000; Carlson and Perdew, 2002; Denison et al., 2002; Yao et al., 2003). In a simplified model of signal transduction, ligand binding to the AHR stimulates its translocation from the cytoplasm to the nucleus, where the receptor heterodimerizes with another PAS protein known as the Ah receptor nuclear translocator (ARNT). This heterodimeric complex recognizes "dioxin-responsive enhancers" within the genome and transactivates a battery of genes that includes those encoding phase I and II biotransformation enzymes (Nebert et al., 2000; Swanson, 2002). Many of the same ligands that activate the AHR are also metabolized by AHR-regulated gene products, which has led to the idea that the physiological role of this pathway is to provide a mechanism by which cells can respond to a variety of structurally related xenobiotic ligands (Ma, 2001; Hahn, 2002; Denison and Nagy, 2003).

In addition to its role in xenobiotic metabolism, the AHR also plays an important role in normal vascular biology and liver development (Yao et al., 2003). The most reproducible and penetrant phenotypes found in *Ahr* mutant mice are smaller adult liver size and the persistence of a fetal vascular shunt known as the ductus venosus (DV) (Fernandez-Salguero et al., 1995; Schmidt et al., 1996; Mimura et al., 1997; Lahvis et al., 2000, 2005; Bunger et al., 2003; Walisser et al., 2004a). In the $Ahr^{-/-}$ mouse model, the patent DV correlates with additional adult phenotypes, including subtle vascular abnormalities in the eye and kidney, as well as cardiomegaly and hypertension as these mice age (Fernandez-Salguero et al., 1995; Schmidt et al., 1996; Lahvis et al., 2000; Thackaberry et al., 2002; Lund et al., 2003). What has not been clear from these earlier studies is the identity of the primary event mediated by the AHR during development. That is, we do not know which of these developmental defects are secondary and which are primary.

We have begun to test the idea that the patent DV observed in adult *Ahr* mutant mice is a secondary effect stemming from a requirement for this protein in early hepatic development. Given that the AHR is expressed in the hepatic primordium by embryonic day (E) 13.5, we predicted that defects might exist in the development of livers from $Ahr^{-/-}$

This work was supported by National Institutes of Health grants P01-CA022484, P30-CA014520, and T32-CA009681.
Article, publication date, and citation information can be found at http://molpharm.aspetjournals.org.
doi:10.1124/mol.105.020107.

ABBREVIATIONS: AHR, aryl hydrocarbon receptor; PAS, Per-Arnt-Sim; ARNT, *Ah* receptor nuclear translocator; DV, ductus venosus; E, embryonic day; FITC, fluorescein isothiocyanate; Pd, postnatal day; MW, molecular weight.

mice and that these earlier aberrations may be causally related to postpartum DV patency (Jain et al., 1998). To test this idea, we performed a detailed survey of hepatovascular development in $Ahr^{-/-}$ mice. Our results are consistent with the idea that the AHR regulates hepatovascular blood flow as early as E15.5 and that this early defect is the cause of patent DV, smaller liver size and hepatic deformation in adult $Ahr^{-/-}$ mice.

Materials and Methods

Mice. Mice congenic for the $Ahr^{\Delta 2}$-null allele were previously generated in this laboratory (Schmidt et al., 1996). This null mouse, hereafter designated $Ahr^{-/-}$, has been backcrossed for 20 generations to the C57BL6/J background (Schmidt et al., 1996). Cohorts of mice heterozygous ($Ahr^{+/-}$) and homozygous ($Ahr^{-/-}$) for the null allele were generated by intercrossing $Ahr^{-/-}$ male mice with $Ahr^{+/-}$ female mice. Our previous work has established that $Ahr^{+/-}$ mice are indistinguishable from $Ahr^{+/+}$ mice with regard to liver development and reproductive biology (Schmidt et al., 1996; Lahvis et al., 2000). Thus, age-matched mice of either genotype, $Ahr^{+/-}$ or $Ahr^{+/+}$, serve as control mice for these studies, as indicated. When needed, age-matched C57BL6/J mice were obtained from The Jackson Laboratory (Bar Harbor, ME). All mice were housed on corncob bedding at 70 ± 2°F with a 12-h light/dark cycle. Mice were fed laboratory mouse chow (LabDiet, Richmond, IN) and water ad libitum.

Hepatic Development in $Ahr^{-/-}$ Mice. Fetal mice were obtained from timed breeding of $Ahr^{+/-}$ female mice with $Ahr^{-/-}$ male mice as described previously (Thomae et al., 2004). In brief, the morning after mating was considered E0.5. Dams were sacrificed by cervical dislocation between E13.5 and E18.5. Each fetus was harvested, placed on ice for anesthesia, and decapitated to ensure death. For each time point, at least nine fetuses of each genotype were analyzed. The fetal abdomens were incised, and the external surface of each liver was visually inspected. When present, the size and location of necrotic lesions were recorded. Each fetus was fixed in 10% (v/v) neutral buffered formalin for 24 h and stored in 70% ethanol for later sectioning. Tissue sections from each developmental time were prepared at 5 μm, stained with hematoxylin and eosin, and subjected to histological examination.

Perfusion of Fetal Livers. Female $Ahr^{+/-}$ and male $Ahr^{-/-}$ mice were bred as described above. Pregnant dams were anesthetized with urethane (urethane, 10 mg/kg i.p.) and warmed on a 37°C heating pad. Each fetus (representing E15.5 through E18.5) was individually removed from the uterus and yolk sac, but the umbilical cord was left attached to the uterus to maintain fetal viability. Each fetus remained in utero until just before injection. To visualize the hepatic vasculature, a solution of fluorescein isothiocyanate (FITC)-labeled dextran (10 mg/ml; Sigma, St. Louis, MO) was injected into the cranial artery on each side (20 μl per injection). The high molecular weight fluor was allowed to perfuse the entire fetus for approximately 2 min to ensure maximal perfusion of the liver. Dye perfusion was confirmed by presence of dye in the superficial vessels of the hind paw and tail vein. After perfusion, abdominal skin, muscle, and peritoneum were removed to expose the liver for in situ imaging. Liver surfaces were flattened for photography using standard Corning 22 × 22-mm glass slipcovers. Livers were imaged using a Leica MZ FLIII with a Leica GFP2 filter set (Leica Microsystems AG, Wetzlar, Germany). Images were captured with a Zeiss AxioCam MRc and viewed and processed with the Zeiss Axiovision 3.1 software package (Carl Zeiss GmbH, Vienna, Austria).

Hepatic Deformation in Adult $Ahr^{-/-}$ Mice. Eight-week-old male $Ahr^{+/+}$, $Ahr^{+/-}$, and $Ahr^{-/-}$ mice ($n = 4$) were anesthetized with urethane (10 mg/kg i.p.), an anesthetic with minimal effects upon the vasculature (Janssen et al., 2004). Livers were perfused via the portal vein with isotonic saline at a rate of 2.5 ml of saline/min for 5 min to ensure maximal exsanguination. Livers were then removed and weighed. Individual hepatic lobes were separated and weighed. Data are expressed as absolute weights of individual lobes. Ratio of left to median lobe weights (L:M ratio) were determined in a larger group of mice ($n = 9$, 13, and 15 for $Ahr^{+/+}$, $Ahr^{+/-}$, and $Ahr^{-/-}$ mice, respectively, representing three independent experiments). In addition, postnatal livers ($n = 6$–9 per age and genotype) were collected from 0-, 1-, 2-, 4-, and 8- week old $Ahr^{+/-}$ and $Ahr^{-/-}$ mice. Individual lobe weights were recorded and presented as L:M ratio.

Portal Vein Morphology. Adult $Ahr^{+/+}$ and $Ahr^{-/-}$ mice (8 weeks old) were anesthetized and dissected to reveal the portal vein. Portal vein diameters were determined using digital calipers at three points in vivo: first, at the emergence from the pancreas, second, inferior to the porta hepatis, and third, halfway between the first two points. For each portal vein, the three measurements were averaged to represent a mean venous diameter. Portal diameter was also determined in postnatal day 1 mice (Pd1) mice. Portal diameter was quantified using the measurement functions within the Zeiss Axiovision 3.1 software package (Carl Zeiss GmbH).

For histological analysis, portal veins were perfused as described above and then fixed in situ by a brief perfusion with neutral buffered formalin. Portal veins were removed from mice with a portion of the Teflon catheter remaining inserted to retain appropriate in vivo length of the vein throughout tissue processing (~50 mm section, 24-gauge Angiocath; BD Infusion Therapy Systems, Inc., Sandy, UT). Venous sections were visualized using standard light microscopy and transmission electron microscopy methods (Thomae et al., 2004).

Immunohistochemistry. Smooth muscle cells were identified using a rabbit anti-human smooth muscle actin primary antibody (Lab Vision Corp., Fremont, CA) and a biotinylated goat ant-rabbit secondary antibody (Jackson ImmunoResearch Laboratories, Inc., West Grove, PA). Biotin moieties were identified using Vectastain ABC methods with NovaRed horseradish peroxidase substrate according to the manufacturer's instructions (Vector Laboratories, Burlingame, CA). Sections were then lightly counterstained with hematoxylin (Fisher Scientific, St. Louis, MO).

Statistics. All data were analyzed using a Student's t test or two-way analysis of variance followed with a Duncan's multiple range test as applicable. Acceptable level of significance was chosen to be $p < 0.05$.

Results

Ontogeny of Fetal Hepatic Necrosis. The livers of littermate $Ahr^{+/-}$ and $Ahr^{-/-}$ mice were examined at E13.5 through postnatal day 2 (Pd2) developmental time points. Representative views from E18.5 mice are shown in Fig. 1. Although livers from $Ahr^{+/-}$ mice appeared normal (Fig. 1A), livers from $Ahr^{-/-}$ littermates commonly exhibited peripheral necrotic lesions (Fig. 1B). These lesions were most prominent in the ventral peripheries of the left lobe and left portion of the median lobe.

The incidence of hepatic necrosis was quantified in $Ahr^{+/-}$ and $Ahr^{-/-}$ mice from E13.5 through Pd2 (Fig. 1C). Livers from $Ahr^{-/-}$ mice were indistinguishable from $Ahr^{+/-}$ at E13.5 and E14.5. As early as E15.5, $Ahr^{-/-}$ mice exhibited signs of peripheral hepatic necrosis. The single observed focus (1 of 39 $Ahr^{-/-}$ fetuses examined) was located in the periphery of the left lobe and was barely discernible upon gross examination (<1 mm^2). Between E16.5 and E17.5, lesions increased in frequency (9 of 34 and 6 of 23, respectively) and were grossly identifiable by a pale appearance, peripheral localization, and clear delineation from the healthy hepatic tissue. The size of these lesions ranged from small foci (<1 mm^2) to larger lesions, often encompassing the peripheral edge of the left and left portion of the median

lobes. At E18.5, the incidence of necrotic lesions continued to increase (18 of 35 mice). Again, the severity of the lesions also varied, ranging from small foci to larger lesions, similar to those observed at E17.5. Again, these lesions were consistently located in the peripheries of the left and median lobes. Compared with earlier time points, the E18.5 lesions appeared much whiter and were more sharply delineated from the remainder of the lobe. In addition, the necrotic lesions composed a larger portion of each lobe, extending into the central regions. The largest lesions observed included up to half of the affected lobe. After birth, the incidence of necrotic lesions increased slightly (13 of 22 mice at Pd1, and 11 of 16 mice at Pd2). However, there was no longer an increase in their severity. Lesions resolved in the first two weeks with occasional residual scarring persisting into adulthood. Control mouse livers appeared normal and showed no signs of hepatic necrosis at any developmental time.

Histology of E18.5 Livers. Histological examination of the lesions observed in $Ahr^{-/-}$ mice indicated segmental necrosis with acute inflammation (Fig. 2B). Hepatocytes within the lesions exhibited eosinophilic cytoplasm, pyknotic nuclei, and loss of cellular boundaries (Fig. 2D). The hepatic capsule commonly contained the entire necrotic lesions, thus maintaining integrity of the liver. In addition to necrotic lesions, livers of $Ahr^{-/-}$ mice exhibited increased extramedullary hematopoiesis with increased populations of end-stage neutrophils, erythrocytes, and myeloid precursors near central veins (Fig. 2F). In addition, bile ducts appear distended and more numerous, with increased mitosis as well as increased nucleus to cytoplasm ratios (data not shown).

Perfusion of Fetal Livers. Fetal livers were perfused with a 2×10^6 molecular weight (MW) FITC-dextran to determine the extent of hepatic perfusion in fetal livers. The high MW of the FITC-dextran was chosen to limit renal clearance of the fluorescent dye. In preliminary experiments, lower MW FITC-labeled dextrans were rapidly cleared by the kidneys and thus were unsuitable for hepatic imaging (data not shown). After injection, each fetus was dissected for hepatic observation using both light and epifluorescence microscopy. This procedure allowed gross visualization of the liver as well as FITC-dextran perfusion of the fetal hepatic vasculature. In most cases, gross appearances of E15.5 livers were indistinguishable between $Ahr^{+/-}$ and $Ahr^{-/-}$ mice under standard light microscopic examination. However, although FITC-dextran penetrated all areas of $Ahr^{+/-}$ livers at E15.5 (Fig. 3A), the fluor failed to fully perfuse the peripheries of the left lobes of the corresponding $Ahr^{-/-}$ livers (Fig. 3B). At E18.5, $Ahr^{+/-}$ livers retained a normal gross appearance and perfused fully. As expected, $Ahr^{-/-}$ livers with necrotic lesions failed to perfuse these areas, demonstrated by the lack of fluorescence in those areas (data not shown).

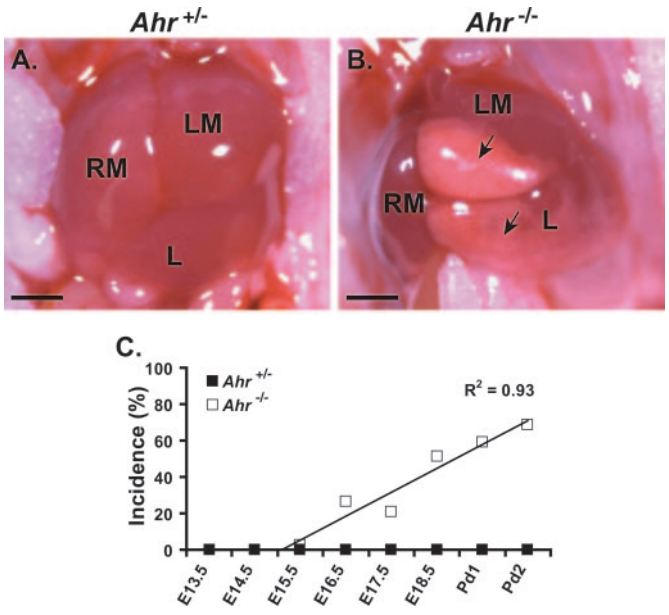

Fig. 1. Hepatic necrosis in fetal $Ahr^{-/-}$ mice. A, $Ahr^{+/-}$ mice exhibit a normal gross hepatic morphology in mice at E18.5 (scale bar, 1 mm). B, livers from E18.5 $Ahr^{-/-}$ mice contain necrotic lesions (arrows) on the peripheries of the left and left median lobes. C, littermate fetuses and pups ($Ahr^{+/-}$ female $\times$ $Ahr^{-/-}$ male, n = 16–39 per age and genotype) were examined for gross appearance of necrosis between E13.5 and Pd1. The endpoint of necrosis in $Ahr^{-/-}$ mice is variable in age of onset as well as magnitude of the necrotic lesion. Data are presented as percentage incidence of $Ahr^{-/-}$ mice in which hepatic necrosis was evident, regardless of magnitude of lesion. LM, left median lobe; RM, right median lobe; L, left lobe.

Altered Liver Morphology in Adult $Ahr^{-/-}$ Mice. Livers from 8-week-old male $Ahr^{+/+}$, $Ahr^{+/-}$, and $Ahr^{-/-}$ mice were dissected. Whole liver and individual lobe weights were recorded and relative lobe weight ratio to whole liver was determined (Fig. 4, A–D). On average, $Ahr^{-/-}$ livers were approximately 31% smaller than livers from $Ahr^{+/+}$ and $Ahr^{+/-}$ mice (0.82 ± 0.02 g, 1.20 ± 0.14 g, and 1.19 ± 0.16 g, respectively). Left lobe weights in $Ahr^{-/-}$ mice were 47 to 50% of $Ahr^{+/+}$ and $Ahr^{+/-}$ left lobe weights (0.18 ± 0.07 g, 0.38 ± 0.04 g, and 0.41 ± 0.06 g, respectively). Although misshapen, weights of the median lobes of $Ahr^{-/-}$ were not statistically different from median lobes of $Ahr^{+/+}$ and $Ahr^{+/-}$ mice (0.37 ± 0.06 g, 0.36 ± 0.05 g, and 0.35 ± 0.05 g, respectively). Right anterior and right posterior lobes were weighed together and determined to be 0.19 ± 0.01 g in $Ahr^{-/-}$ mice compared with 0.33 ± 0.06 g and 0.33 ± 0.05 g in $Ahr^{+/+}$ and $Ahr^{+/-}$ mice, respectively. Caudate lobes were also smaller in $Ahr^{-/-}$ mice (0.10 ± 0.01 g, 0.10 ± 0.0 g, and 0.05 ± 0.01 g in $Ahr^{+/+}$, $Ahr^{+/-}$, and $Ahr^{-/-}$ caudate lobes, respectively). Representative whole livers and individual lobes from $Ahr^{+/+}$ and $Ahr^{-/-}$ mice are shown in Fig. 4, B and C. Whole livers from $Ahr^{-/-}$ mice were noticeably smaller than wild-type control mice. Visual inspection revealed that the left lobes of $Ahr^{-/-}$ mice had markedly distinct morphology compared with their corresponding controls. Livers from $Ahr^{+/+}$ and $Ahr^{+/-}$ were visibly indistinguishable (data not shown).

Because of the consistency in absolute lobe weight, median lobes provided a stable internal reference for relative lobe weights (Fig. 4D). Comparison of left-to-median-lobe-weight ratios (1.08 ± 0.05, 1.10 ± 0.03, and 0.60 ± 0.04 for $Ahr^{+/+}$, $Ahr^{+/-}$, and $Ahr^{-/-}$ mice, respectively) illustrates that the L:M ratios for $Ahr^{+/+}$ and $Ahr^{+/-}$ do not differ. However, the L:M ratio for $Ahr^{-/-}$ mice is significantly less than either $Ahr^{+/+}$ and $Ahr^{+/-}$ ratios. Thus, the L:M ratio served as a biomarker which clearly distinguishes *Ahr* genotype from both $Ahr^{+/+}$ and $Ahr^{+/-}$. In an additional experiment, the relative left to median lobe weight (L:M) ratio was quantified from Pd1 through 8 weeks of age (Fig. 4E). At Pd1, the L:M ratio was indistinguishable in $Ahr^{+/-}$ and $Ahr^{-/-}$ mice (0.76 ± 0.04 and 0.67 ± 0.03, respectively). All other ages displayed a differential L:M ratio. In $Ahr^{+/+}$ mice, the L:M ratios increased with age (e.g., at 1, 2, 4, and 8 weeks, the

L:M ratio was 0.92 ± 0.02, 0.92 ± 0.06, 1.0 ± 0.09, and 1.08 ± 0.04, respectively). In $Ahr^{-/-}$ mice, the L:M ratios decreased slightly at 1, 2, 4, and 8 weeks (0.62 ± 0.06, 0.67 ± 0.08, 0.59 ± 0.06, and 0.64 ± 0.06, respectively).

Portal Vein Morphology. Portal vein diameter was assessed in situ in anesthetized 8-week-old $Ahr^{+/-}$ and $Ahr^{-/-}$ mice (Fig. 5, A and B). Average portal diameter in $Ahr^{-/-}$ was significantly ($p < 0.05$) greater than $Ahr^{+/-}$ mice (Fig. 5C, 1.52 ± 0.27 mm and 0.84 ± 0.23 mm, respectively). Portal vein diameter was also assessed in situ in anesthetized Pd1 $Ahr^{+/-}$ and $Ahr^{-/-}$ mice (Fig. 5, D and E). Average portal diameter in $Ahr^{-/-}$ did not differ significantly ($p < 0.05$) from $Ahr^{+/-}$ mice (Fig. 5F, 0.41 ± 0.10 mm and 0.33 ± 0.10 mm, respectively).

Portal veins from $Ahr^{+/-}$ and $Ahr^{-/-}$ mice were qualitatively assessed. Trichrome-stained sections indicated that portal veins of $Ahr^{-/-}$ mice have less smooth muscle than control mice (Fig. 6, A and B). This was confirmed by immunohistochemical staining for smooth muscle actin (Fig. 6, C and D), as well as by histological examination of smooth muscle cells by TEM (Fig. 6, E and F). In contrast, smooth muscle cellularity of hepatic arteries was indistinguishable between $Ahr^{+/-}$ and $Ahr^{-/-}$ mice (Fig. 6, A–D). Transmission electron microscopy confirmed the decreased smooth muscle

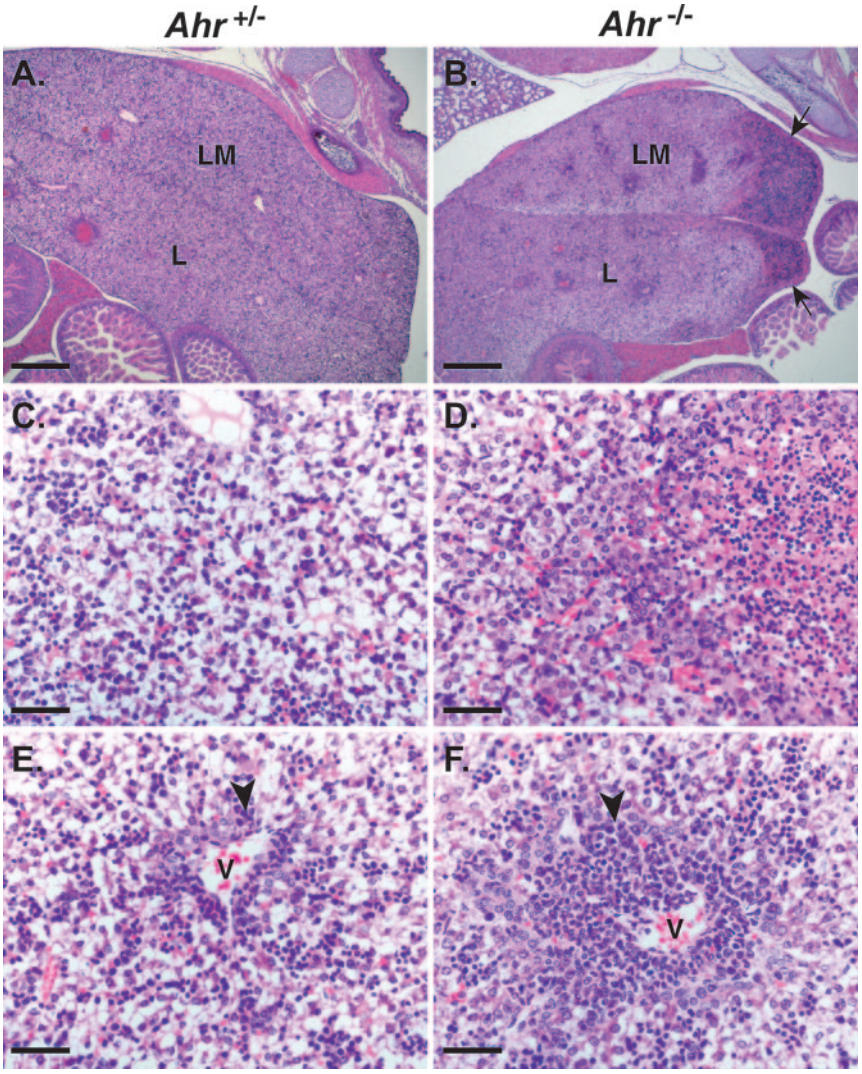

Fig. 2. Histological phenotype in fetal $Ahr^{-/-}$ mice. A and B, histological examination of E18.5 $Ahr^{+/-}$ and $Ahr^{-/-}$ mice, respectively, confirms the presence of necrotic lesions (arrows) at the periphery of left and left median lobes of $Ahr^{-/-}$ livers (bar = 500 μm). C and D, normal fetal parenchyma is observed in $Ahr^{+/-}$ mice (C, scale bar, 50 μm). However, necrosis is clearly evident in the peripheral regions of $Ahr^{-/-}$ mice (D, right side of frame). E and F, extramedullary hematopoiesis (arrowheads) is present in both strains of mice but is more extensive in $Ahr^{-/-}$ mice (F, scale bar, 50 μm). LM, left median lobe; RM, right median lobe; L, left lobe; V, vein.

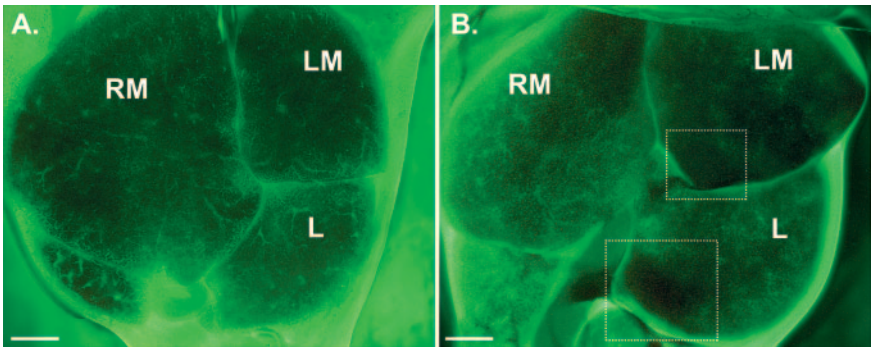

Fig. 3. Hepatic perfusion in fetal $Ahr^{+/-}$ and $Ahr^{-/-}$ mice. A and B, livers from littermate $Ahr^{+/-}$ and $Ahr^{-/-}$ fetuses were examined at E15.5 for FITC-dextran perfusion of the parenchyma (scale bars, 1 mm). Note that fetal livers were flattened with a slipcover to facilitate imaging. A, livers from E15.5 $Ahr^{+/-}$ fetuses were completely perfused (magnification, 2.5×). B, livers from E15.5 $Ahr^{-/-}$ fetuses did not fully perfuse in the peripheries of the left lobe and the left median lobe (boxes). LM, left median lobe; RM, right median lobe; L, left lobe.

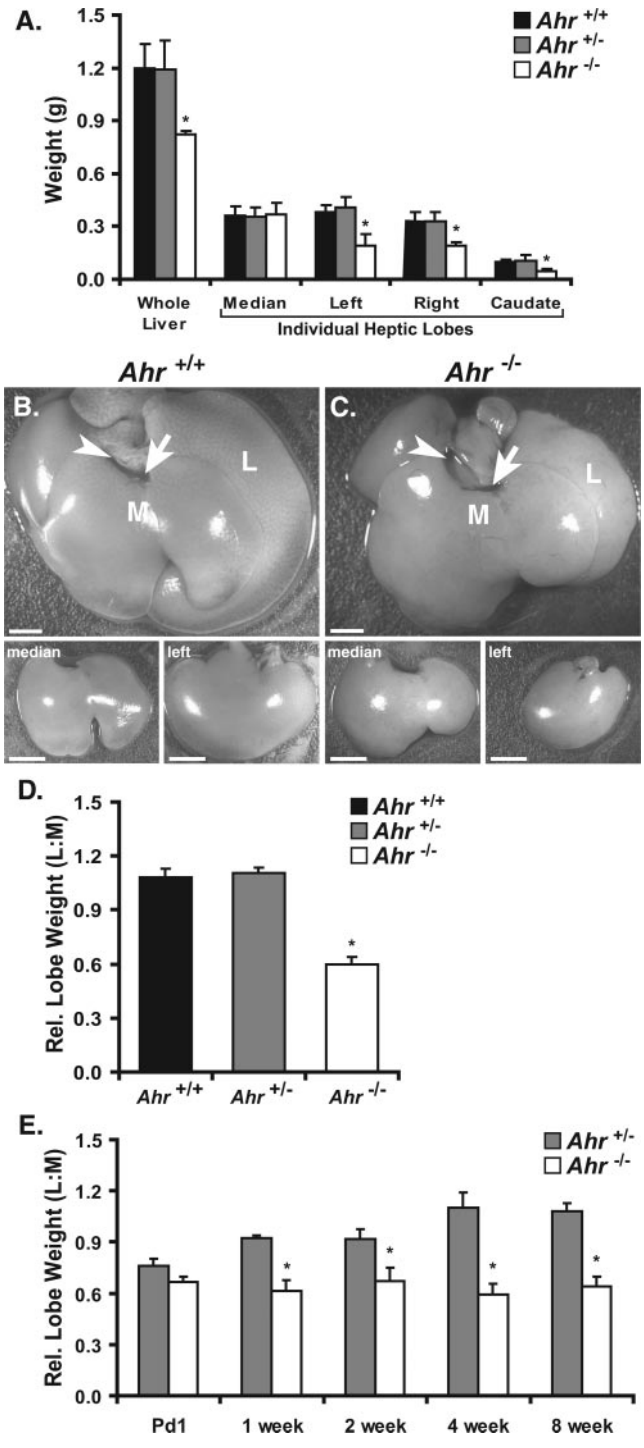

Fig. 4. Hepatic morphology in adult $Ahr^{-/-}$ mice. A, livers from 8-week-old male $Ahr^{+/+}$, $Ahr^{+/-}$, and $Ahr^{-/-}$ mice were dissected and weighed to determine the contribution of each lobe to the total liver weight. Whole livers from $Ahr^{-/-}$ mice were significantly smaller than either $Ahr^{+/+}$ or $Ahr^{+/-}$ livers because of smaller left, right, and caudate lobes. Median lobe weight did not differ among the three genotypes. B and C, representative wild-type ($Ahr^{+/+}$) and $Ahr^{-/-}$ livers with suprahepatic IVC (arrowhead) and efferent hepatic vein indicated (arrow; scale bars, 3 mm). Insets, dissected median and left hepatic lobes from $Ahr^{+/+}$ and $Ahr^{-/-}$ mice (scale bars, 5 mm). Note the decreased size of the left lobe from the $Ahr^{-/-}$ liver. Although similar in weight, the left ventral portion of the $Ahr^{-/-}$ median lobe appeared to be atrophied with contralateral compensation. D, the relative left to median (L:M) lobe weight ratio served as a biomarker to discriminate wild-type ($Ahr^{+/+}$ and $Ahr^{+/-}$) from $Ahr^{-/-}$ genotypes. E, individual hepatic lobes from ≤8-week old $Ahr^{+/+}$ and $Ahr^{-/-}$ mice were separated and weighed. The L:M ratio illustrated the component, yet indicated no significant morphological difference in the endothelial cells between $Ahr^{+/-}$ and $Ahr^{-/-}$ mice.

Discussion

Several reports have demonstrated that the AHR plays an important role in normal liver biology. Smaller liver size is the most consistent phenotype reported for three independently generated null alleles of the *Ahr* locus (Fernandez-Salguero et al., 1995; Schmidt et al., 1996; Mimura et al., 1997). It has been our working hypothesis that the smaller liver size is a result of a persistent portocaval shunt known as the ductus venosus (Lahvis et al., 2000, 2005; Bunger et al., 2003; Walisser et al., 2004a). The DV is a fetal intrahepatic vessel that connects the umbilical vein and the portal vein to the vena cava during fetal development, thereby allowing nutrient-rich umbilical blood to flow directly into systemic circulation with minimal perfusion of the hepatic parenchyma (Kiserud, 1999). Normally, this shunt closes between 24 and 48 h after birth; whereas, in *Ahr* mutant mice, the DV remains patent for the lifespan of the animal (Lahvis et al., 2005). It follows, but it has not been proven, that $Ahr^{-/-}$ mice have smaller livers because the patent DV diverts normal blood flow from the hepatic sinusoids resulting in decreased hepatic nutrient and subsequent liver atrophy.

The signaling pathway by which the AHR regulates DV closure seems to be similar to the pathway by which this receptor regulates xenobiotic metabolism and the hepatotoxic response to dioxins. These processes require nuclear localization of the AHR and heterodimerization with ARNT (Bunger et al., 2003; Walisser et al., 2004a,b). Mice with a mutation in the nuclear translocation signal of the AHR ($Ahr^{nls/nls}$) maintain capacity for agonist binding yet do not display dioxin-induced up-regulation of xenobiotic metabolizing gene products, dioxin-induced hepatotoxicity, and closure of the DV (Bunger et al., 2003). A role for the *Arnt* locus in AHR-dependent DV closure is derived from the observation that mice harboring a hypomorphic *Arnt* allele ($Arnt^{fxneo/fxneo}$) also display a patent DV (Walisser et al., 2004b). Our interpretation of these data is that the formation of the AHR-ARNT complex is an essential step in the response to xenobiotic chemicals and in the regulation of vascular development.

Adult $Ahr^{-/-}$ mice display additional, more subtle, vascular defects, including a persistent hyaloid artery and a confused vasculature of the corneal limbus (Schmidt et al., 1996; Fernandez-Salguero et al., 1997; Lahvis et al., 2000; Lund et al., 2003). Similar to the DV, the hyaloid artery of the eye functions in organ perfusion during gestation and resolves after parturition (Saint-Geniez and D'Amore, 2004). Adult $Ahr^{-/-}$ mice have also been reported to exhibit age-dependent hypertension and cardiac hypertrophy by 5 months of age (Fernandez-Salguero et al., 1997; Thackaberry et al., 2002). The mechanism behind this cardiac pathology has

onset of the adult $Ahr^{-/-}$ phenotype. At Pd1, the L:M ratio did not differ because of the weight contribution of the necrotic tissue. Within two weeks of age, these lesions resolved resulting in stunted left lobe growth which persists throughout maturation. Data were analyzed using a one- and two-way analysis of variances with a Duncan's multiple range test. Acceptable level of significance was chosen to be $p < 0.05$. M, median lobe; L, left lobe.

been suggested to involve cardiac hypoxia and elevated serum angiotensin-II, as captopril treatment prevented the hypertensive and cardiac effects (Thackaberry et al., 2002; Lund et al., 2003). Overall, these observations represent an emerging pattern of AHR-dependent anatomical and physiological changes that lead us to suggest that the AHR pathway plays an important role in normal vascular biology.

Given that AHR expression is first detectable in the livers of mice by E13.5, we suspected that this receptor system might be acting early in hepatic development (Jain et al., 1998). It was our hypothesis that patent DV and decreased liver weight observed post partum were secondary phenotypes that arose from an earlier defect in $Ahr^{-/-}$ mouse liver development. Careful inspection of fetal mice revealed peripheral hepatic necrosis in $Ahr^{-/-}$ livers as early as E15.5 (Figs. 1 and 2). Examination of additional gestational time points revealed that the incidence of necrosis increased with age. By birth most $Ahr^{-/-}$ mice had distinct necrotic lesions in the lobar peripheries. These observations support our hypothesis that AHR plays an important role in hepatovascular development during gestation.

The presence of necrotic lesions in lobe peripheries led us to examine whether these regions were receiving diminished blood flow in $Ahr^{-/-}$ livers (Kerr et al., 1972; Jaeschke and Lemasters, 2003). To test this idea, we employed a fluorescent dye to assess the regional perfusion of the hepatic parenchyma of $Ahr^{+/-}$ and $Ahr^{-/-}$ at E15.5 and E18.5. These time points were chosen as they represent the prenecrotic $Ahr^{-/-}$ liver and the maximal presentation of the fetal necrotic lesions, respectively. It is noteworthy that peripheries of E15.5 and E18.5 $Ahr^{-/-}$ livers were resistant to perfusion. Resistance to perfusion was particularly noteworthy in the E15.5 liver, because this developmental time rarely presents with regional necrosis (Fig. 3). As expected in E18.5 $Ahr^{-/-}$ mice, decreased peripheral perfusion localized with necrotic lesions. Thus, peripheral resistance to perfusion is more likely to be the cause of the later necrosis, rather than the necrosis-preventing perfusion. Taken in sum, these data are consistent with the idea that the primary hepatic defect in $Ahr^{-/-}$ mice involves decreased peripheral perfusion of the emergent liver as early as E15.5.

The early hepatovascular events and hepatic necrosis occurring in the $Ahr^{-/-}$ fetus seem to explain the altered liver morphology observed in adult animals. The left, caudate, and right lobes are approximately half the weight of their wild-type counterparts, whereas the median lobes are relatively similar in weight (Fig. 4). It is noteworthy that although the overall weight of the median lobe did not differ, it was misshapen. The left half of the median lobe appeared atrophied with apparent compensation in the right half. This observation could not be quantified as the median lobe cannot be consistently bisected. However, the observations of atrophy and compensation within the median lobe explain the unchanged lobe weight. We used stability of the median lobe weight as an internal reference point to calculate the left-to-median-lobe-weight ratio (L:M). This ratio consistently remains near 1.0 and 0.5 for wild-type and $Ahr^{-/-}$ mice, respectively, resulting in a simple method to determine genotype in future studies. Overall, the aberrant lobe weights in $Ahr^{-/-}$ livers were consistent with the observed lobe specificity of fetal necrosis and aberrant perfusion. These observations are the first demonstration of altered liver lobe morphology in $Ahr^{-/-}$ mice. In addition, the L:M ratio provides an anatomic biomarker that easily discriminates between wild-type and $Ahr^{-/-}$ genotypes. These data are consistent with a model in which aberrations in the perfusion of the specific hepatic lobes lead to permanent alterations in adult liver morphology.

Although we do not yet understand the mechanism that underlies the observed altered hepatic perfusion, it is tempting to speculate that this phenotype is secondary to increased sinusoidal resistance leading to portal hypertension during liver development. In our previous work, we have noted malformed sinusoidal patterns in the adult $Ahr^{-/-}$ liver (Lahvis et al., 2000). These anastomotic sinusoids may impede hepatic blood flow resulting in both the inhibition of peripheral perfusion and the commensurate back pressure that prevents closure of the DV. On the other hand, increased peripheral resistance could be secondary to physical block to blood flow as a result of increased populations of hematopoietic cells observed within the developing $Ahr^{-/-}$ liver (Fig. 2; Schmidt et al., 1996). Whichever mechanism underlies this

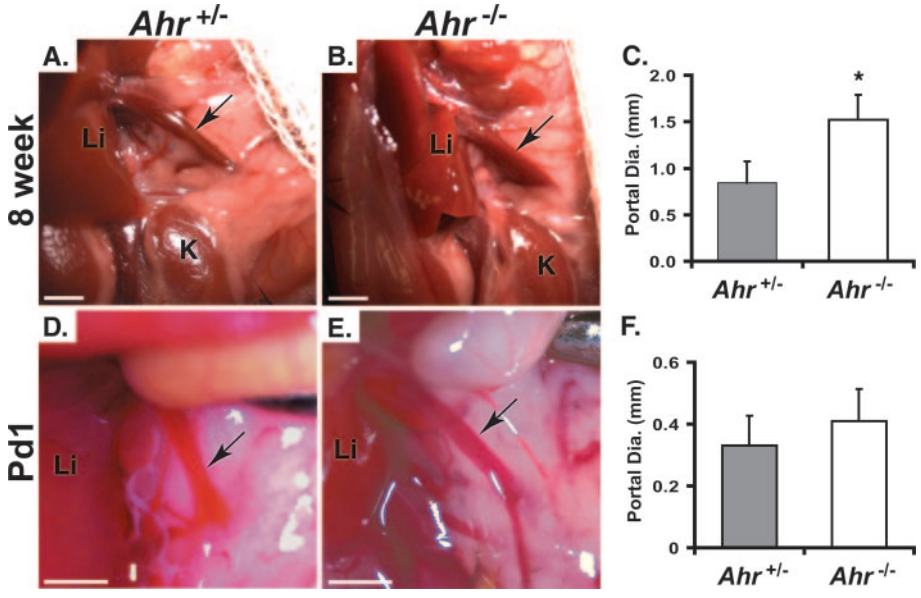

Fig. 5. Portal diameter in adult $Ahr^{+/-}$ and $Ahr^{-/-}$ mice. A and B, portal vein diameter was assessed in situ in anesthetized adult $Ahr^{+/-}$ and $Ahr^{-/-}$ mice, respectively (scale bars, 3 mm). Portal veins (arrows) were larger in $Ahr^{-/-}$ mice, relative to $Ahr^{+/-}$ mice. D and E, portal vein diameter was also assessed in situ in anesthetized $Ahr^{+/-}$ and $Ahr^{-/-}$ mice at Pd1, respectively (scale bars, 1 mm). Portal veins (arrows) were indistinguishable in $Ahr^{-/-}$ mice and $Ahr^{+/-}$ mice. C, average diameter of portal veins in adult $Ahr^{+/-}$ and $Ahr^{-/-}$ mice. F, average diameter of portal veins in Pd1 $Ahr^{+/-}$ and $Ahr^{-/-}$ mice. Data were analyzed using a Student's t test with significance at $p < 0.05$. Li, liver; K, kidney.

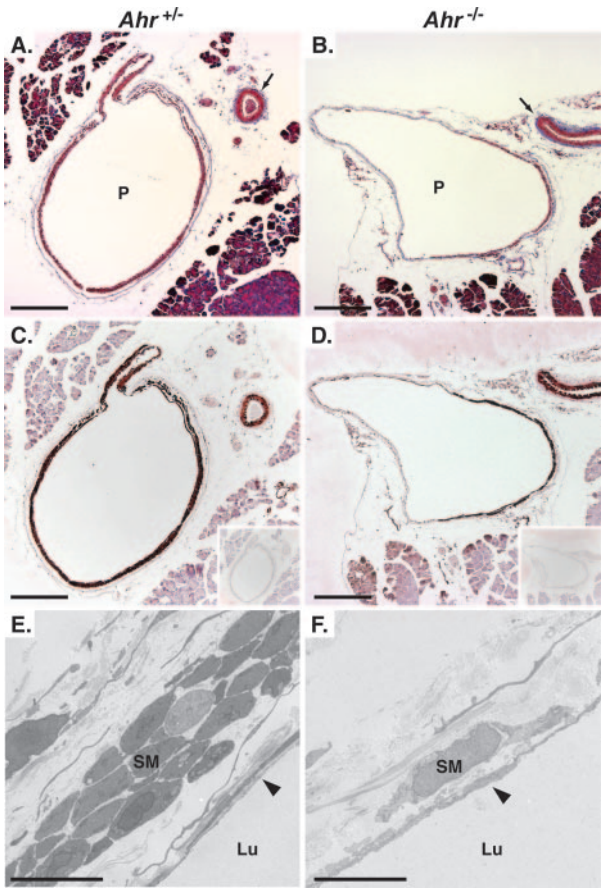

Fig. 6. Portal histology in adult $Ahr^{+/-}$ and $Ahr^{-/-}$ mice. A and B, trichrome-stained sections from $Ahr^{+/-}$ and $Ahr^{-/-}$ mice show less smooth muscle in portal veins from $Ahr^{-/-}$ mice (scale bars, 200 μm). Hepatic arteries do not differ between $Ahr^{+/-}$ and $Ahr^{-/-}$ mice (arrows). C and D, immunostaining for α-smooth muscle actin confirms the identity of smooth muscle cells in $Ahr^{+/-}$ and $Ahr^{-/-}$ mice (insets, antibody controls, bars = 200 μm). E and F, TEM images from $Ahr^{+/-}$ and $Ahr^{-/-}$ mice show no apparent difference in the endothelial cells (arrowheads, 3400× magnification; scale bars, 5 μm). However, fewer smooth muscle cells are present in representative sections. P, portal vein; Lu, lumen; SM, smooth muscle cell.

impaired perfusion, the resultant necrotic lesions in the $Ahr^{-/-}$ liver would explain the altered lobe morphology in the adult $Ahr^{-/-}$ mouse liver.

At the present time, it is difficult to provide a mechanistic link between the early peripheral resistance to hepatic blood flow and the later presentation of a patent DV in the adult animal. We speculate that the patent DV might be the result of increased portal pressure during late gestation and that this increased pressure inhibits closure of the shunt during a crucial perinatal window. Although these data provide support for the existence of increased resistance to hepatic blood flow, the proof of a causal relationship is not conclusive. Given that direct measurements of portal pressure cannot be assessed in the developing mouse liver, we attempted an indirect measurement of portal hypertension (i.e., diameter of the portal vein) (Fig. 5). The portal vein diameter is similar between perinatal wild-type and $Ahr^{-/-}$ mice, consistent previous reports (Lahvis et al., 2005). In contrast, the portal veins of adult $Ahr^{-/-}$ mice are significantly larger than those of control mice. In addition, the smooth muscle layer surrounding the portal vein was found to be discontinuous and thinner overall (Fig. 6). Taken together, these observations suggest either a failed maturation of pericytes or a pressure overload during portal vein maturation. Whereas these data support a model of DV patency secondary to embryonic perfusion abnormalities, it will be important in the future to test a causal relationship directly.

These data provide evidence that the AHR has an essential physiological role in liver vascular development that appears as early as E15.5. Our data indicate that hepatic necrosis, altered liver morphology, and, possibly, DV patency may be secondary to a common AHR-related defect in early vascular development. These data are consistent with a model in which altered blood flow through the parenchyma results in regional necrosis, which has a permanent affect on liver lobe morphology and patency of the DV. In turn, these early hepatovascular defects lead to a number of physiological and morphological changes in the adult mouse.

References

Bunger MK, Moran SM, Glover E, Thomae TL, Lahvis GP, Lin BC, and Bradfield CA (2003) Resistance to 2,3,7,8-tetrachlorodibenzo-*p*-dioxin toxicity and abnormal liver development in mice carrying a mutation in the nuclear localization sequence of the aryl hydrocarbon receptor. *J Biol Chem* **278:**17767–17774.

Carlson DB and Perdew GH (2002) A dynamic role for the *Ah* receptor in cell signaling? Insights from a diverse group of *Ah* receptor interacting proteins. *J Biochem Mol Toxicol* **16:**317–325.

Denison MS and Nagy SR (2003) Activation of the aryl hydrocarbon receptor by structurally diverse exogenous and endogenous chemicals. *Annu Rev Pharmacol Toxicol* **43:**309–334.

Denison MS, Pandini A, Nagy SR, Baldwin EP, and Bonati L (2002) Ligand binding and activation of the *Ah* receptor. *Chem Biol Interact* **141:**3–24.

Fernandez-Salguero P, Pineau T, Hilbert DM, McPhail T, Lee SS, Kimura S, Nebert DW, Rudikoff S, Ward JM, and Gonzalez FJ (1995) Immune system impairment and hepatic fibrosis in mice lacking the dioxin-binding Ah receptor. *Science (Wash DC)* **268:**722–726.

Fernandez-Salguero PM, Ward JM, Sundberg JP, and Gonzalez FJ (1997) Lesions of aryl-hydrocarbon receptor-deficient mice. *Vet Pathol* **34:**605–614.

Gu Y-Z, Hogenesch J, and Bradfield C (2000) The PAS superfamily: sensors of environmental and developmental signals. *Annu Rev Pharmacol Toxicol* **40:**519–561

Hahn ME (2002) Aryl hydrocarbon receptors: diversity and evolution. *Chem Biol Interact* **141:**131–160.

Jaeschke H and Lemasters JJ (2003) Apoptosis versus oncotic necrosis in hepatic ischemia/reperfusion injury. *Gastroenterology* **125:**1246–1257.

Jain S, Maltepe E, Lu MM, Simon C, and Bradfield CA (1998) Expression of ARNT, ARNT2, HIF1 alpha, HIF2 alpha and *Ah* receptor mRNAs in the developing mouse. *Mech Dev* **73:**117–123.

Janssen BJ, De Celle T, Debets JJ, Brouns AE, Callahan MF, and Smith TL (2004) Effects of anesthetics on systemic hemodynamics in mice. *Am J Physiol* **287:** H1618–H1624.

Kerr JF, Wyllie AH, and Currie AR (1972) Apoptosis: a basic biological phenomenon with wide-ranging implications in tissue kinetics. *Br J Cancer* **26:**239–257.

Kiserud T (1999) Hemodynamics of the ductus venosus. *Eur J Obstet Gynecol Reprod Biol* **84:**139–147.

Lahvis G, Lindell S, Thomas R, McCuskey R, Murphy C, Glover E, Bentz M, Southard J, and Bradfield C (2000) Portosystemic shunts and persistent fetal vascular structures in *Ah*-receptor deficient mice. *Proc Natl Acad Sci USA* **97:** 10442–10447.

Lahvis GP, Pyzalski RW, Glover E, Pitot HC, McElwee MK, and Bradfield CA (2005) The aryl hydrocarbon receptor is required for developmental closure of the ductus venosus in the neonatal mouse. *Mol Pharmacol* **67:**714–720.

Lund AK, Goens MB, Kanagy NL, and Walker MK (2003) Cardiac hypertrophy in aryl hydrocarbon receptor null mice is correlated with elevated angiotensin II, endothelin-1 and mean arterial blood pressure. *Toxicol Appl Pharmacol* **193:**177–187.

Ma Q (2001) Induction of CYP1A1. The AhR/DRE paradigm: transcription, receptor regulation and expanding biological roles. *Curr Drug Metab* **2:**149–164.

Mimura J, Yamashita K, Nakamura K, Morita M, Takagi TN, Nakao K, Ema M, Sogawa K, Yasuda M, Katsuki M, et al. (1997) Loss of teratogenic response to 2,3,7,8-tetrachlorodibenzo-p-dioxin (TCDD) in mice lacking the *Ah* (dioxin) receptor. *Genes Cells* **2:**645–654.

Nebert DW, Roe AL, Dieter MZ, Solis WA, Yang Y, and Dalton TP (2000) Role of the aromatic hydrocarbon receptor and [*Ah*] gene battery in the oxidative stress response, cell cycle control and apoptosis. *Biochem Pharmacol* **59:**65–85.

Saint-Geniez M and D'Amore PA (2004) Development and pathology of the hyaloid, choroidal and retinal vasculature. *Int J Dev Biol* **48:**1045–1058.

Schmidt JV, Su GH, Reddy JK, Simon MC, and Bradfield CA (1996) Characterization of a murine *Ahr* null allele: involvement of the *Ah* receptor in hepatic growth and development. *Proc Natl Acad Sci USA* **93:**6731–6736.

Swanson HI (2002) DNA binding and protein interactions of the AHR/ARNT heterodimer that facilitate gene activation. *Chem Biol Interact* **141:**63–76.

Thackaberry EA, Gabaldon DM, Walker MK, and Smith SM (2002) Aryl hydrocarbon receptor null mice develop cardiac hypertrophy and increased hypoxia-inducible factor-1alpha in the absence of cardiac hypoxia. *Cardiovasc Toxicol* **2:**263–274.
Thomae TL, Glover E, and Bradfield CA (2004) A maternal *Ahr* null genotype sensitizes embryos to chemical teratogenesis. *J Biol Chem* **279:**30189–30194.
Walisser JA, Bunger MK, Glover E, and Bradfield CA (2004a) Gestational exposure of *Ahr* and *Arnt* hypomorphs to dioxin rescues vascular development. *Proc Natl Acad Sci USA* **101:**16677–16682.
Walisser JA, Bunger MK, Glover E, Harstad EB, and Bradfield CA (2004b) Patent ductus venosus and dioxin resistance in mice harboring a hypomorphic *Arnt* allele. *J Biol Chem* **279:**16326–16331.
Yao GH, Harstad EB, and Bradfield CA (2003) *PAS Proteins: Regulators and Sensors of Development and Physiology*, Kluwer Academic Publishers, Boston.

Address correspondence to: Dr. Christopher A. Bradfield, McArdle Laboratory for Cancer Research, 1400 University Avenue, Madison, WI 53711. E-mail: bradfield@oncology.wisc.edu